Distinct modes of centromere protein dynamics during cell cycle progression in *Drosophila* S2R+ cells

Peter V. Lidsky[1,*], Frank Sprenger[2] and Christian F. Lehner[1,‡]

[1]Institute of Molecular Life Sciences (IMLS), University of Zurich, Zurich CH-8057, Switzerland
[2]Institute of Genetics, University of Regensburg, 93053 Regensburg, Germany

*Present address: Institute of Gene Biology, Russian Academy of Sciences, Moscow 119334, Russia
‡Author for correspondence (christian.lehner@imls.uzh.ch)

Accepted 15 July 2013
Journal of Cell Science 126, 4782–4793

doi: 10.1242/jcs.134122

Summary

Centromeres are specified epigenetically in animal cells. Therefore, faithful chromosome inheritance requires accurate maintenance of epigenetic centromere marks during progression through the cell cycle. Clarification of the mechanisms that control centromere protein behavior during the cell cycle should profit from the relatively simple protein composition of *Drosophila* centromeres. Thus we have analyzed the dynamics of the three key players Cid/Cenp-A, Cenp-C and Cal1 in S2R+ cells using quantitative microscopy and fluorescence recovery after photobleaching, in combination with novel fluorescent cell cycle markers. As revealed by the observed protein abundances and mobilities, centromeres proceed through at least five distinct states during the cell cycle, distinguished in part by unexpected Cid behavior. In addition to the predominant Cid loading onto centromeres during G1, a considerable but transient increase was detected during early mitosis. A low level of Cid loading was detected in late S and G2, starting at the reported time of centromere DNA replication. Our results reveal the complexities of *Drosophila* centromere protein dynamics and its intricate coordination with cell cycle progression.

Key words: Centromere, Cid, Cenp-A, Cenp-C, Cal1, Cell cycle, Mitosis, S phase, *Drosophila*

Introduction

Accurate chromosome segregation during mitotic and meiotic divisions depends on functional centromeres. Chromosomes lacking centromere function fail to assemble kinetochores and cannot be integrated properly into the spindle. Similarly, chromosomes with ectopic extra centromeres frequently fail to arrive at a bipolar orientation within the spindle. Therefore, it is crucial for genetic stability that one and only one functional centromere per chromosome is maintained during progression through division cycles.

With the notable exception of budding yeast, centromeres are specified epigenetically (Black and Cleveland, 2011). A centromere-specific variant of histone H3 is thought to play a crucial role in the epigenetic marking of centromere identity. The first example Cenp-A was identified in human cells (Earnshaw and Rothfield, 1985). Homologs have been observed in essentially all eukaryotes. The *Drosophila* ortholog has been named centromere identifier (Cid) (Blower and Karpen, 2001; Henikoff et al., 2000). Targeting of Cid to ectopic sites using a *lacO-lacI* system is sufficient for neocentromere formation (Mendiburo et al., 2011), whereas Cid depletion leads to chromosome loss (Blower and Karpen, 2001; Raychaudhuri et al., 2012). In the following comments on Cenp-A homologs from various species, these will be designated CenH3 proteins for convenience, although this term is not unproblematic (Earnshaw et al., 2013).

The structure of CenH3 nucleosomes *in vivo* is not yet clear. It might be quite different from that of canonical octameric nucleosomes and depend on species and cell cycle stage (reviewed by Padeganeh et al., 2013a; Nechemia-Arbely et al., 2012). However, octameric nucleosomes with CenH3 instead of histone H3 can be assembled readily *in vitro* and these CenH3 nucleosomes do not have a strong preference for specific DNA sequences (Carroll et al., 2009; Tachiwana et al., 2011; Kingston et al., 2011; Dechassa et al., 2011). Moreover, characterization of neocentromeres has provided further evidence that the intrachromosomal localization of Cenp-A is not dictated by specific DNA sequences (Barry et al., 1999; du Sart et al., 1997; Amor et al., 2004; Alonso et al., 2010).

The analysis of the mechanisms that control CenH3 deposition on chromosomes and restrict its localization to the centromeric region is in progress. Strong overexpression of *cid* in *Drosophila* can overcome the localization restraint, resulting in misincorporation into chromosome arm regions. Interestingly, misincorporated Cid is rapidly degraded (Moreno-Moreno et al., 2011; Moreno-Moreno et al., 2006). Similar findings were made in yeast (Ranjitkar et al., 2010; Hewawasam et al., 2010). However, despite clearance of misincorporated Cid, ectopic centromeres are formed occasionally after high levels of *cid* overexpression, resulting in chromosome missegregation and genetic instability (Olszak et al., 2011; Heun et al., 2006).

In addition to elimination of misincorporated CenH3, a dedicated loading machinery appears to direct CenH3 deposition specifically to the centromeric region. Loading of CenH3 on centromeres is tightly interconnected with cell cycle control (Black and Cleveland, 2011). In human cells, centromeric recruitment of newly synthesized Cenp-A occurs exclusively during exit from mitosis and early G1 (Jansen et al., 2007),

whereas in S and G2 it is prevented by Cdk activity (Silva et al., 2012). Cenp-A deposition is a complex multistage process known to engage diverse factors (for a review, see Nechemia-Arbely et al., 2012). Before the actual loading of newly synthesized Cenp-A, centromeres have to be licensed (or primed) in a process that depends on the Mis18 complex (Fujita et al., 2007; Silva et al., 2012; Moree et al., 2011; Dambacher et al., 2012; Hayashi et al., 2004). Subsequent Cenp-A recruitment during early G1 is dependent on the loading factor HJURP (Foltz et al., 2009; Dunleavy et al., 2009), which is distantly related to yeast Scm3 (Mizuguchi et al., 2007; Camahort et al., 2007; Sanchez-Pulido et al., 2009). Incorporation of recruited Cenp-A into chromatin is thought to depend on Rsf-1 (Perpelescu et al., 2009) and maturation into stable centromeric nucleosomes later in G1 involves MgcRacGAP (Lagana et al., 2010). Thereafter, Cenp-A has been reported to remain stable at the centromere without any detectable turn-over (Hemmerich et al., 2008; Mellone et al., 2011; Jansen et al., 2007).

Although the control of CenH3 deposition in non-human organisms usually shares some similarities with that of Cenp-A described above, some clear differences have also been revealed. In fission yeast, CenH3 recruitment was shown to occur in both S and G2 (Takayama et al., 2008). In *Arabidopsis*, CenH3 deposition takes place mainly during G2 (Lermontova et al., 2006). Evidence from *Drosophila* has revealed developmental stage- and cell-type-specific control. In early embryos, Cid loading occurs during exit from mitosis in anaphase (Schuh et al., 2007). In neuroblasts, Cid is recruited somewhat later – during early G1 (Dunleavy et al., 2012). In spermatocytes, it occurs during the extended G2 phase before meiosis (Raychaudhuri et al., 2012; Dunleavy et al., 2012). Finally, in cultured *Drosophila* cells, Cid has been proposed to be recruited in metaphase when Cdk activity is high (Mellone et al., 2011).

Apart from the reported differences in the time of CenH3 loading, a surprising divergence has also evolved in the cast of proteins implicated in centromere specification and propagation. For example, out of more than 20 proteins that form the constitutive centromere-associated network (CCAN) in mammalian cells, only Cenp-A/Cid and Cenp-C appear to be present in *Drosophila* and *C. elegans* (Heeger et al., 2005; Moore and Roth, 2001; Perpelescu and Fukagawa 2011; McAinsh and Meraldi, 2011). Similarly, a Mis18bp homolog cannot be identified in *Drosophila*, and Cal1 the putative functional *Drosophila* equivalent of HJURP/Scm3 shares so little sequence similarity that it has been proposed to reflect convergent evolution (Phansalkar et al., 2012).

The reduced complexity of the *Drosophila* centromere makes this organism an effective model for the analysis of centromere maintenance during the cell cycle. Localization of the few centromere components Cid, Cenp-C and Cal1 has been shown to be interdependent (Goshima et al., 2007; Erhardt et al., 2008; Schittenhelm et al., 2010). Cid serves as an epigenetic centromere mark (Mendiburo et al., 2011; Raychaudhuri et al., 2012), Cenp-C as a structural platform for kinetochore assembly in mitosis (Przewloka et al., 2011; Gascoigne et al., 2011) and Cal1 is proposed to function as a Cid loading factor rather than serving a structural role (Phansalkar et al., 2012; Schittenhelm et al., 2010). Importantly, analyses in *Drosophila* have revealed that the maintenance mechanisms preserve not only the chromosomal location of centromeric Cid, but also its amount. Experimentally enforced alterations in the level of centromeric Cid in sperm are maintained during development of the next generation (Raychaudhuri et al., 2012). Acute overloading of Cid at centromeres during embryonic cell division cycles causes severe mitotic defects (Schittenhelm et al., 2010), emphasizing the relevance of quantitative control.

For further characterization of the mechanisms of centromere maintenance, we analyzed the dynamics of Cid, Cenp-C and Cal1 in cultured *Drosophila* S2R+ cells. Using quantitative *in vivo* imaging and fluorescence recovery after photobleaching (FRAP), we demonstrate unexpected complexities in the behavior of these proteins and identify a series of distinct centromere states during progression through the cell cycle.

Results

S2R+ cell lines coexpressing fluorescent centromere proteins and cell cycle markers

To evaluate the effects of progression through the cell cycle on centromere protein dynamics, we established stable S2R+ cell lines expressing a fluorescent version of a given centromere protein (Cid, Cenp-C or Cal1) in combination with proteins allowing cell cycle stage assignment (Fig. 1). The fluorescent centromere protein variants were previously shown to be functional (Schuh et al., 2007; Schittenhelm et al., 2010; Schittenhelm et al., 2009). Expression of these variants was controlled by the cis-regulatory regions of the corresponding centromere protein genes (Fig. 1A). For cell cycle stage assignment, mCherry-PCNA was used either alone or in combination with a cyclin B (CycB) fragment (aa 1–285) fused with an HA-tag and a nuclear localization signal at its N-terminal end, and with EBFP2 at its C-terminal end (HAnlsCycB$^{1–285}$-EBFP2) (Fig. 1A,B). Expression of cell cycle markers was driven by the metallothionein promoter (Bunch et al., 1988), allowing graded expression by varying the copper sulfate concentration in the culture medium.

Pulse labeling with the thymidine analogue 5-ethynyl-2′-deoxyuridine (EdU) confirmed that S phase was accompanied by the expected change in the intranuclear pattern of mCherry-PCNA signals (Shermoen et al., 2010; Leonhardt et al., 2000). In early S phase, EdU and mCherry-PCNA signals were present throughout the nucleus in a fine granular pattern. In late S phase, these signals were enriched in bright clusters restricted to a subnuclear region closely associated with the nucleoli (Fig. 1C). The characteristic transition from the early fine granular mCherry-PCNA distribution to the late clusters was also apparent during live imaging (Fig. 1D). Although the change from a homogenous to granular mCherry-PCNA appearance during the G1–S transition could not be detected unambiguously in every cell, it was often clearly apparent, as illustrated in the last column in Fig. 1D, where one of two daughter cells still has a homogenous distribution and the other already has a granular appearance. For quantification of centromere protein intensities during the cell cycle, we only used data from cells displaying an obvious transition. The comparison of mCherry-PCNA with HAnlsCycB$^{1–285}$-EBFP2 signals revealed that the latter protein started to accumulate during S phase, as expected (Lehner and O'Farrell, 1990), reaching peak levels in the nucleus just before mitosis (Fig. 1D). During early mitosis, HAnlsCycB$^{1–285}$-EBFP2 was re-distributed throughout the cell, followed by degradation during exit from mitosis (Fig. 1D). Because degradation was not yet complete in telophase, HAnlsCycB$^{1–285}$-EBFP2 re-accumulated in the re-forming nuclei, followed by further

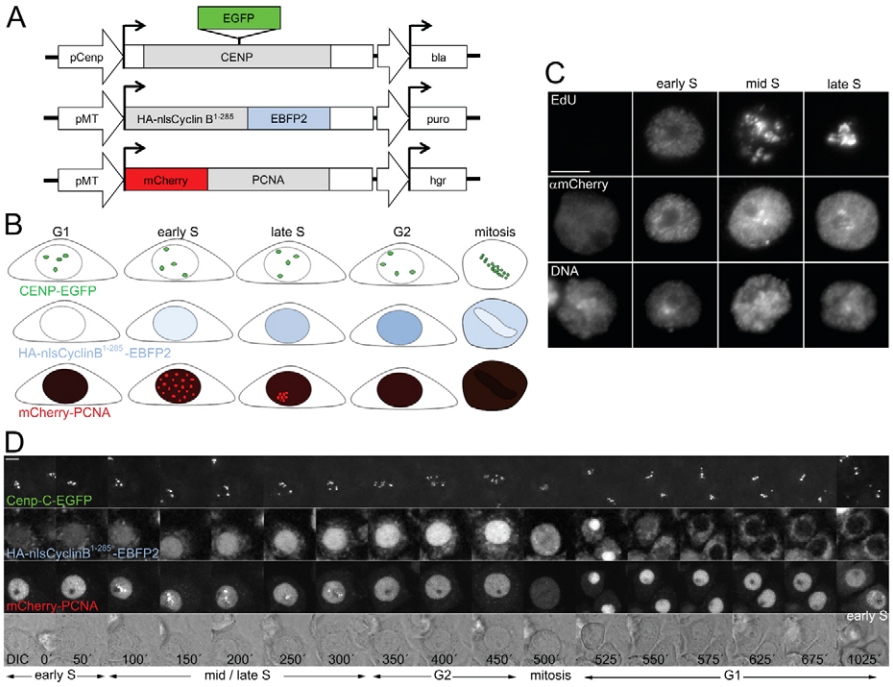

Fig. 1. Cell cycle reporter system. (A) Schematic illustration of the different constructs used for the generation of stably transfected S2R+ cells co-expressing EGFP-tagged centromere proteins (top) and the cell cycle reporters HAnlsCycB$^{1–285}$-EBFP2 (middle) and mCherry-PCNA (bottom). Expression was driven by either the cis regulatory region of the centromere protein genes (pCenp) or the metallothionein promoter (pMT). Selectable marker cassettes (bla, hgr and puro) allowed sequential selection of stable co-expressing transformants. (B) Schematic illustration of the expression of EGFP-tagged centromere proteins (top) and the cell cycle reporters HAnlsCycB$^{1–285}$-EBFP2 (middle) and mCherry-PCNA (bottom) during cell cycle progression. Cells in S phase display granular mCherry-PCNA distribution in the nucleus. Cells in G1 and G2 are differentiated by HAnlsCycB$^{1–285}$-EBFP2 expression. (C) Pulse labeling with EdU confirmed that the intranuclear pattern of mCherry-PCNA reports the DNA replication pattern changes characteristic of progression through S phase (Shermoen et al., 2010). Representative interphase cells are shown that were (from left to right) either not in S phase or during early, mid and late S phase. (D) Time lapse *in vivo* imaging of a representative cell co-expressing Cenp-C-EGFP and the cell cycle reporters HAnlsCycB$^{1–285}$-EBFP2 and mCherry-PCNA. Differential interference contrast (DIC) is shown in the bottom row where time in minutes is also given. Cell cycle stages are indicated below the micrographs. Scale bars: 5 µm.

degradation to background levels within one hour (Fig. 1D). As cells and their nuclei were relatively small during early G1, this cell cycle stage could be discriminated readily from G2 in spite of the relatively slow degradation of HAnlsCycB$^{1–285}$-EBFP2. We point out that the expressed CycB fragment did not include the cyclin box which is required for Cdk1 binding. Signal intensities of both cell cycle markers (mCherry-PCNA and HAnlsCycB$^{1–285}$-EBFP2) were sufficiently strong for long-term live imaging. Moreover, these signals could be separated readily from those of the coexpressed EGFP-Cenp fusions (Fig. 1D, see supplementary material Movie 1 and data not shown). We used additional stably transformed S2R+ cell lines for analyses during mitosis. These cell lines expressed the EGFP-Cenp fusions in combination with metallothionein-promoter-driven histone H2Av-mRFP1 (His2Av-mRFP) (Fig. 2B).

The total amount of centromeric Cid increases during G1

On the basis of recent analyses in *Drosophila* S2 and Kc167 cells, incorporation of a new Cid complement into centromeres was proposed to occur during metaphase (Mellone et al., 2011). This conclusion was based primarily on quench-chase-pulse experiments with SNAP-tagged Cid which reported rapid centromere association of newly synthesized Cid with maximal sensitivity, but limited information concerning incorporation stability. Here, we applied *in vivo* imaging and quantification of Cid-EGFP to monitor centromeric levels during progression through the cell cycle in two different cell lines expressing either mCherry-PCNA (Fig. 2A,C,D) or His2Av-mRFP (Fig. 2B,C). A comparison of the total centromeric Cid-EGFP signal intensities per cell revealed 50% lower levels in early G1 (average of first two frames after mitosis) compared with late G2 (average of last two frames before mitosis) (Fig. 2C). Therefore, centromeric Cid-EGFP levels were directly correlated with the number of centromeres, which is 50% lower in G1 compared with G2. This result is inconsistent with the proposal that Cid incorporation during proliferation of cultured *Drosophila* cells occurs during metaphase. After stable incorporation of a new Cid protein complement into centromeres during metaphase, total centromeric Cid-EGFP signal intensity per cell is expected to be equal before and after mitosis, and not halved by mitosis as revealed by our quantification. Moreover, our signal quantification during cell cycle progression provided additional evidence indicating that incorporation of a new Cid protein complement into centromeres did not happen during metaphase but rather during G1. We clearly detected a significant increase of centromeric Cid-EGFP signals per cell during progression through G1 (Fig. 2C) whereas centromeric Cid-EGFP intensities remained constant throughout S and G2 (Fig. 2D). We emphasize that equivalent results were obtained using two different imaging approaches (see the Materials and Methods).

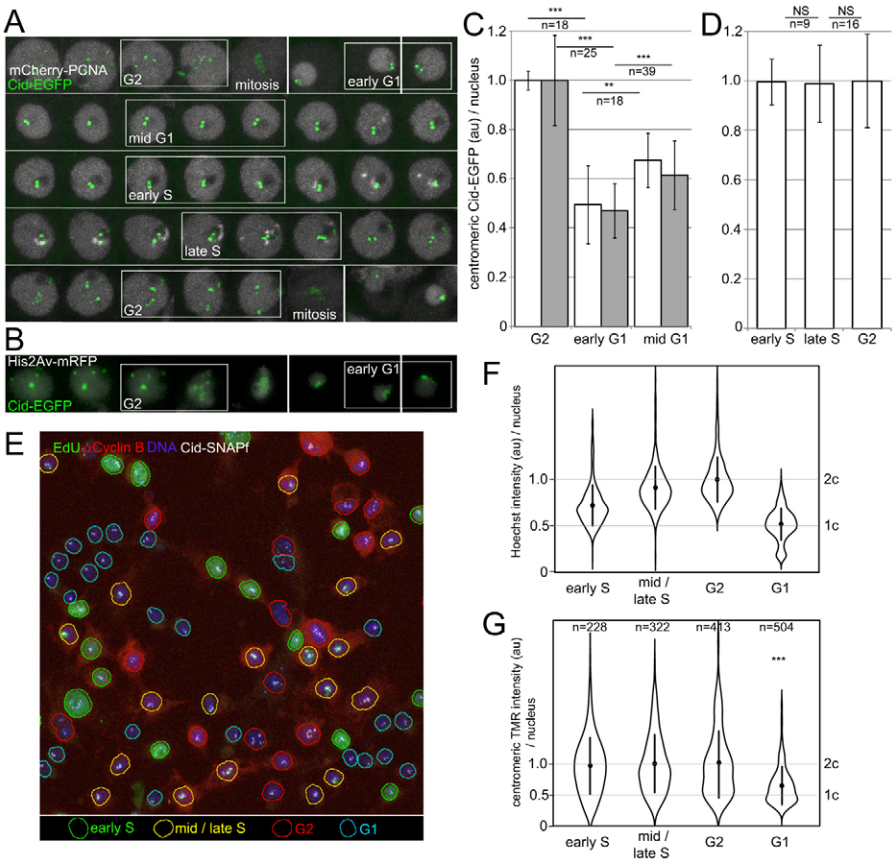

Fig. 2. Amounts of centromeric Cid-EGFP during progression through the cell cycle. (A) *In vivo* imaging was performed with S2R+ cells expressing Cid-EGFP and mCherry-PCNA. Maximum projections of *z* stacks acquired every 30 minutes show a representative cell progressing through the cell cycle from top left to bottom right. Boxed time points were used for quantification of average centromeric Cid-EGFP levels during distinct cell cycle stages (G2, early G1, mid G1, early S, late S; see white bars in C and D). Two time points were used for comparison of late G2 with early G1, and three for comparison of S with G2. (B) *In vivo* imaging was performed with S2R+ cells expressing Cid-EGFP and His2Av-mRFP. Maximum projections of *z* stacks acquired every 20 minutes show a representative cell progressing from G2 through mitosis into G1. Boxed time points were used for quantification of centromeric Cid-EGFP levels before and after mitosis (see gray bars in C). (C,D) Bar diagrams indicating total centromeric Cid-EGFP amounts per cell at distinct cell cycle stages. The number of cells that were analyzed is indicated above the bars. Values were obtained with S2R+ cells expressing Cid-EGFP and either mCherry-PCNA (white bars; see A) or His2Av-mRFP (gray bars; see B). Significant differences were observed between G2 and early G1, as well as between early and mid G1 (**$P<0.01$; ***$P<0.001$). By contrast, no significant differences (NS) were observed between early and late S and between late S and G2. (E,F) S2R+ cells expressing Cid-SNAPf were pulse labeled with EdU followed by TMR-Star labeling. (E) After EdU, DNA and anti-Cyclin B staining, CellProfiler was used to classify cells in G1, early S, mid/late S and G2. (F) Average signal intensity of DNA staining. (G) Average centromeric TMR signal intensities reflecting the amount of centromeric Cid-SNAPf in the different classes. Violin plots with average and s.d. are shown. Quantified cell numbers are given in G. G1 cells have significantly lower TMR signals at centromeres compared with other cell cycle stages (*** $P<0.001$).

For additional confirmation, we generated stably transformed S2R+ cells expressing SNAPf-tagged Cid. This particular Cid variant can be fluorescently labeled by addition of TMR-Star, a tetramethylRhodamine derivative, to the culture medium (Keppler et al., 2004). Quantification after labeling with such a low molecular weight compound appeared preferable to anti-Cid immunolabeling where complications with variable epitope accessibility during different cell cycle stages were encountered. To assign cell cycle stages, we pulse labeled the SNAPf-Cid cells with EdU before TMR-Star addition, and used anti-Cyclin-B and a DNA stain for additional labeling after fixation (Fig. 2E). Cell cycle stages were classified automatically by CellProfiler (Carpenter et al., 2006) (supplementary material Fig. S1). EdU-positive cells were classified as either ‘early S’ or ‘mid/late S’ depending on the projected fraction of the nuclear area occupied by the EdU signal. The total nuclear area was obtained from the DNA channel. EdU-negative cells were classified as G1 or G2 based on anti-CycB signal intensities. Classification quality was validated by analysis of the DNA staining intensities, which had not been exploited for the automatic classification (Fig. 2F). As expected, average DNA signal intensity in the G1 class was 50% of that in the G2 class (Fig. 2F). Moreover, average DNA staining intensity in the early S class was lower than in the mid/late S class, and both these values were in between the G1 and G2 values (Fig. 2F). The observed DNA staining intensities therefore clearly validated our automatic classification. Importantly, the quantification of centromeric Cid-SNAPf signal intensities in the different classes fully confirmed the findings of our previous analyses with Cid-EGFP. Centromeric Cid-SNAPf signals were found to be almost indistinguishable in early S, mid/late S and G2 (Fig. 2G). By contrast, signals in G1 were slightly higher than half of the S and G2 values (Fig. 2G), which is fully consistent with the notion that

the new complement of Cid is incorporated into centromeres during G1.

The increase of centromeric Cid during metaphase is transient

To evaluate whether newly synthesized Cid associates with centromeres also during metaphase in S2R+ cells, as previously observed in S2 and Kc167 cells (Mellone et al., 2011), we performed analogous quench-chase-pulse experiments with our Cid-SNAPf cells and made comparable observations (data not shown). Moreover, after photobleaching of centromeric Cid-EGFP we clearly observed recovery in prometaphase cells (i.e. before anaphase) (Fig. 3A). However, since the comparison of Cid-EGFP in G2 and G1 had failed to reveal persistent Cid incorporation into centromeres during mitosis (Fig. 2C), we hypothesized that association of Cid with centromeres during metaphase is either transient or quantitatively minor in relation to the total centromeric Cid. Attempts to evaluate this issue by *in vivo* imaging of TMR-Star labeled newly synthesized Cid-SNAPf during progression through mitosis failed because of high background signals. Therefore, we performed a careful quantification of centromeric Cid-EGFP signals during mitosis after *in vivo* imaging (Fig. 3B,E). In this manner, an increase in centromeric signals during metaphase was indeed also detected (Fig. 3E). However, during progression through anaphase and telophase, centromeric Cid-EGFP levels were observed to decrease again (Fig. 3E). Normalized by the number of centromeres, centromeric Cid-EGFP increased about 1.4-fold from late G2 to metaphase, but by the time of anaphase and telophase it was again down at the level of late G2 (Fig. 3E). We conclude that the association of Cid with metaphase centromeres is only transient. Alternatively, a persistent incorporation of newly synthesized Cid into centromeres during metaphase remains a possibility, but such stable incorporation would have to be compensated by a commensurate and slightly delayed loss of old Cid during exit from mitosis.

To determine whether Cenp-C displayed a similar dynamic association with metaphase centromeres, we performed analogous analyses with Cenp-C-EGFP (Fig. 3F). Our results indicated that some Cenp-C-EGFP was also recruited to metaphase centromeres. However, in contrast to Cid-EGFP, a complete return of centromeric Cenp-C-EGFP levels back to pre-mitotic levels was not observed during completion of mitosis. Therefore, some Cenp-C appears to be incorporated into centromeres during mitosis.

The extensive and rapid movements of centromeres during mitosis include dissolution of interphase clusters during prophase and close spatial clustering during anaphase and telophase. To address whether spatial dynamics might distort quantification of total centromeric EGFP signals during mitosis, we analyzed additional proteins, Spc25-EGFP and Bub3-EGFP. Spc25 is a component of the essential Ndc80 kinetochore protein complex (Wigge and Kilmartin, 2001; Janke et al., 2001; Schittenhelm et al., 2007). As expected, centromeric Spc25-EGFP signals were found to increase rapidly during kinetochore assembly at the onset of mitosis, but no longer did so from prometaphase to metaphase (Fig. 3C,G). Results concerning Bub3, a spindle assembly checkpoint component, also corresponded to the expectations based on analyses of fixed cells (Taylor et al., 1998; Basu et al., 1998). Bub3-EGFP signals increased rapidly at centromeres during early mitosis but dropped again from prometaphase to metaphase and during exit from mitosis (Fig. 3D,H). We conclude that our quantification of centromeric EGFP signals is unlikely to be grossly distorted by the dynamic changes in the spatial distribution of centromeres during mitosis.

Centromeric Cid dynamics changes in late S phase

To compare the dynamic behavior of centromeric Cid observed during mitosis with that in other cell cycle stages, we performed FRAP experiments using cells expressing mCherry-PCNA in addition to Cid-EGFP. During G1, we observed significant

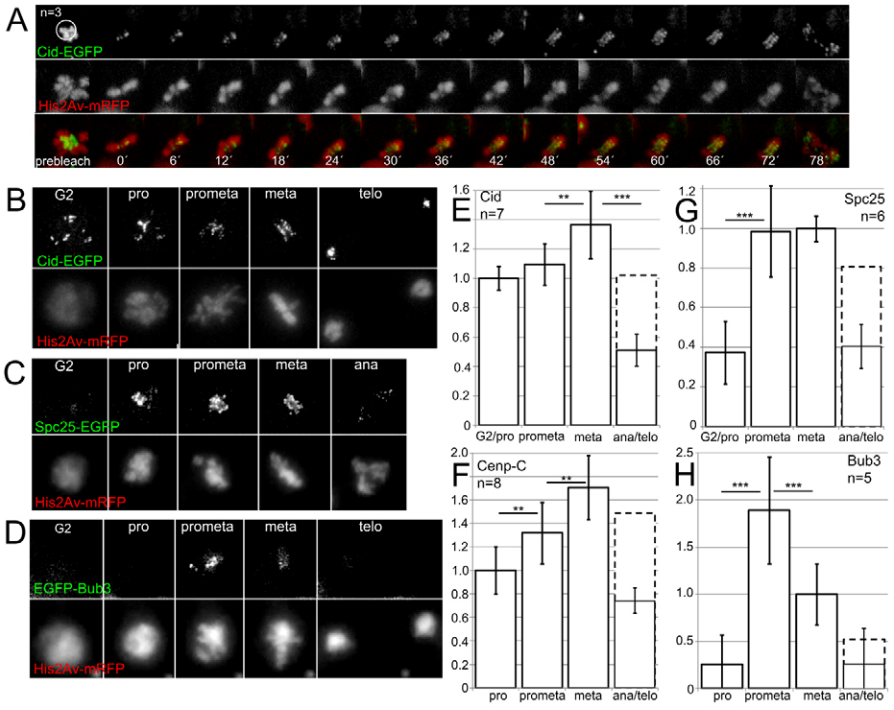

Fig. 3. Centromere and kinetochore protein dynamics during mitosis. (A) FRAP experiment indicating recruitment of Cid-EGFP to the centromere during metaphase. Centromeric Cid-EGFP in S2R+ cells coexpressing His2Av-mRFP was photobleached in prometaphase. Subsequent recovery of centromeric Cid-EGFP signals up to metaphase was clearly apparent. (B–H) Centromeric EGFP signals in S2R+ cells expressing His2Av-mRFP and Cid-EGFP (B), Cenp-C-EGFP (not shown), Spc25-EGFP (C) or EGFP-Bub3 (D) were imaged during progression through mitosis and quantified at different mitotic stages (E–H). Bars and whiskers represent average intensity per cell with s.d. Numbers of analyzed cells (n) are given in E–H. Significant differences are indicated by black lines (**$P<0.01$, ***$P<0.001$). The dashed bars display the double of the solid bars with values obtained during late mitosis (ana/telo) where centromeric EGFP signals per daughter nucleus were measured. These dashed bars allow direct comparisons of levels per centromere to those in the earlier mitotic stages.

recovery after photobleaching of centromeric Cid-EGFP (Fig. 4A). This finding is consistent with the observed increase of total centromeric Cid-EGFP levels during G1 (Fig. 2C) and supports the notion that incorporation of a new complement of Cid into centromeres occurs during G1. By contrast, we failed to detect significant recovery during early S phase (Fig. 4A). Unexpectedly, however, a modest but significant recovery was observed during late S and G2 (Fig. 4B,C). Interestingly, this Cid-EGFP recovery started at the time that corresponds to the reported time of centromere DNA replication in cultured *Drosophila* cells (Sullivan and Karpen, 2001). When centromeres were photobleached in early S phase, recovery did not start until very late in S phase (Fig. 4B,C). Moreover, recovery continued in G2 (Fig. 4B,C). The data displayed in Fig. 4C are from cells that entered mitosis successfully, suggesting that recovery of centromeric Cid-EGFP during late S and G2 is unlikely a result of severe damage induced by initial strong photobleaching pulse. Moreover, onset of recovery was precisely correlated with the S–G2 transition and not with the time point of the initial photobleaching pulse. In addition, at the onset of recovery, centromeres were always colocalized with the PCNA cluster that marks replication factories. All these observations suggest that replication of centromeric DNA induces a state of centromeric chromatin that allows some Cid recruitment.

Cal1 decreases during G1 and reappears around G1/S

Cal1 has been proposed to function as a Cid loading factor (Erhardt et al., 2008; Schittenhelm et al., 2010; Phansalkar et al., 2012). To compare the behavior of Cal1 during cell cycle progression with that of Cid, we performed analyses with Cal1-EGFP cells expressing mCherry-PCNA. In contrast to Cid which is largely confined to the centromere, a substantial fraction of Cal1 is localized at the nucleolus (Schittenhelm et al., 2010; Erhardt et al., 2008). The intimate spatial association of the nucleolus and the centromere clusters that is observed in the great majority of the cells made a separate quantification of centromeric and nucleolar Cal1-EGFP signals difficult. However, signal intensities in the centromere clusters and in the nucleolus appeared to be closely correlated during cell cycle progression and were therefore quantified together. This quantification indicated that Cal1-EGFP levels decreased strongly during progression through G1, followed by rapid re-accumulation around the G1–S transition to levels that remained constant throughout S and G2 phases (Fig. 5A,B). Although Cal1-EGFP signals in the centromere clusters often appeared to be still slightly above the nucleolar signals, even when overall signals were minimal, we cannot exclude the possibility that the ratio between centromeric and nucleolar signals might change during progression through interphase.

To analyze the mobility of centromeric Cal1-EGFP, we performed FRAP experiments. For these experiments, we selected cells in which at least one of the centromere clusters was well separated from the nucleolus. After photobleaching such centromere clusters, Cal1-EGFP signals recovered rapidly within few minutes to pre-bleach values (Fig. 5D,E). Recovery dynamics and extent was comparable during G1, S and G2 phases (supplementary material Fig. S2). Photobleaching within the nucleolar region resulted in a decrease of centromeric Cal1-EGFP signals, with dynamics comparable to recovery after centromere bleaching (supplementary material Fig. S2), indicating that nucleolar and centromeric Cal1-EGFP pools are in rapid exchange. Therefore, centromeric Cal1 appears to be far more dynamic than Cid (Fig. 4) and Cenp-C (see below). This

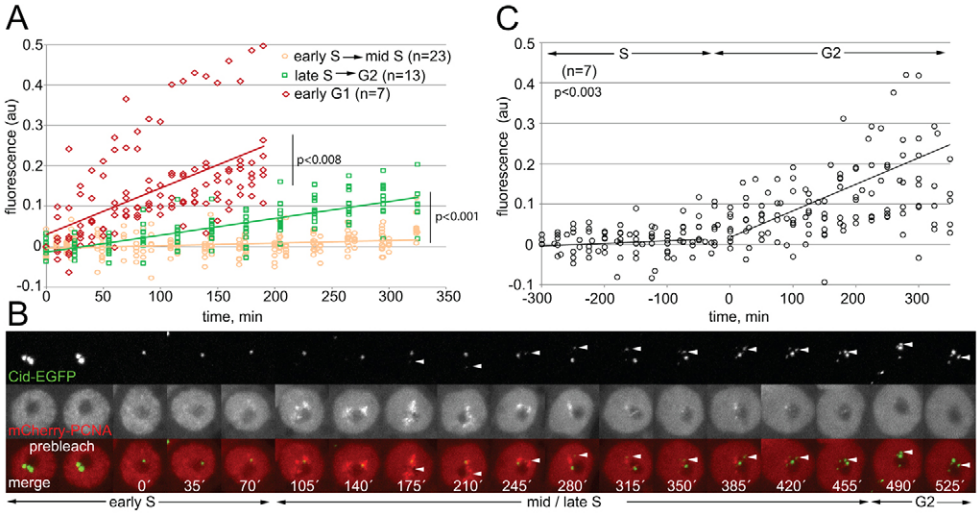

Fig. 4. A change in mobility of centromeric Cid-EGFP in late S phase. (A–C) Centromeric Cid-EGFP in S2R+ cells coexpressing either His2Av-mRFP (red diamonds in A) or mCherry-PCNA (all other data) was photobleached and recovery of centromeric EGFP signals was analyzed over time. Maximal recovery was seen after photobleaching in G1 (red diamonds in A; two out of seven analyzed cells displayed faster recovery and one cell was not analyzed beyond 70 minutes). By contrast, no recovery was detected initially after photobleaching in early S (beige circles in A). Unexpectedly, however, limited recovery was observed after photobleaching in late S (green squares in A). Moreover, such limited recovery was also observed after photobleaching in early S, but only when analyses were extended beyond progression through late S, as illustrated with a representative example (B) and by quantification of a total of seven cells (C). Although no recovery occurred initially, it started eventually late in S, as indicated by arrowheads (B) and by an increase in the recovery slope during the S–G2 transition (C). The recovery measurements of the seven analyzed cells were superimposed using the last time point in S (final frame with mCherry-PCNA cluster) for temporal registration.

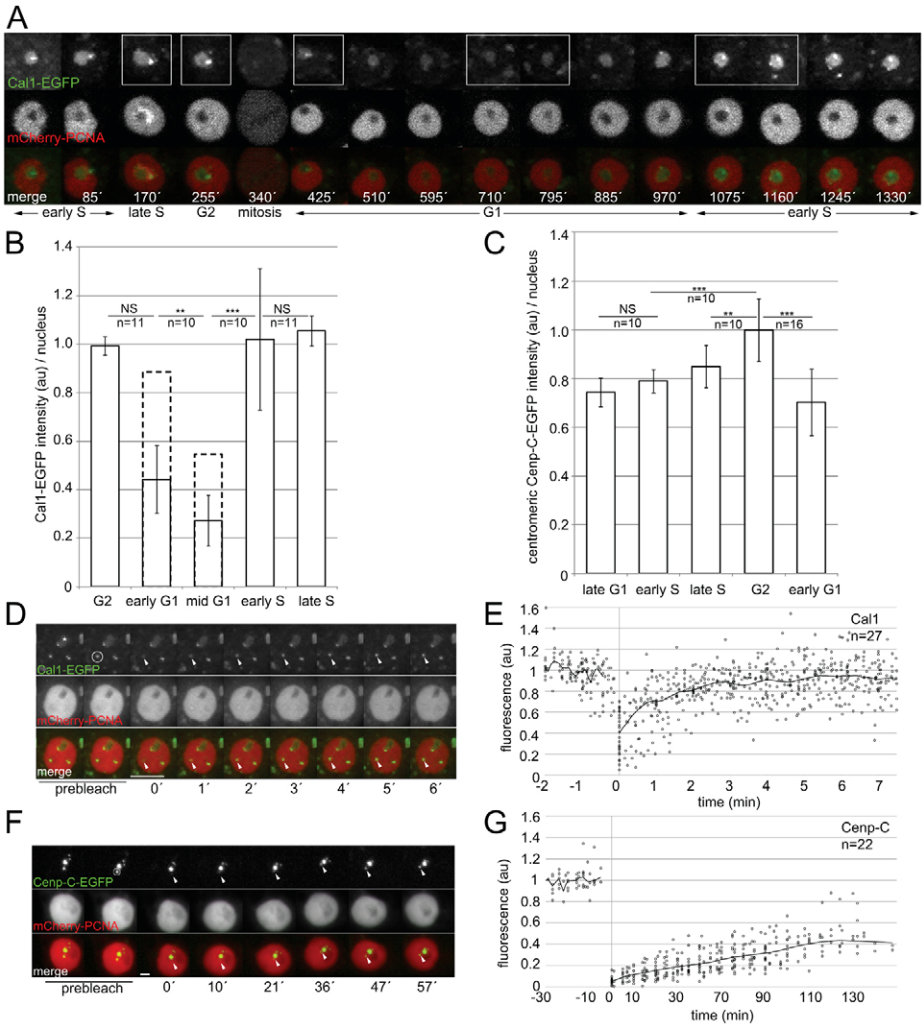

Fig. 5. Cal1 and Cenp-C behavior during the cell cycle. (A,B) Cal1-EGFP levels. S2R+ cells expressing Cal1-EGFP and the cell cycle reporters mCherry-PCNA and HAnlsCycB$^{1–285}$-EBFP2 (not shown) were analyzed by time-lapse *in vivo* imaging. Cal1-EGFP signal per cell was quantified at defined cell cycle stages (boxed in A). Average intensities (± s.d., n indicated above bars) are displayed in B. No significant change (NS) was brought about by progression through mitosis, as revealed by the comparison of G2 with G1 after normalization to account for the difference in centromere number per cell (bars with dashed line). By contrast, significant disappearance during G1 and re-accumulation around G1–S was readily apparent (**P<0.01, ***P<0.001). (C) Centromeric Cenp-C-EGFP levels. S2R+ cells expressing Cenp-C-EGFP and the cell cycle reporters mCherry-PCNA and HAnlsCycB$^{1–285}$-EBFP2 were analyzed by time lapse *in vivo* imaging followed by quantification of centromeric EGFP signals at defined cell cycle stages. (D,E) Cal1-EGFP FRAP. Centromeric Cal1-EGFP in cells coexpressing mCherry-PCNA and HAnlsCycB$^{1–285}$-EBFP2 (not shown) was photobleached (circle in D) during G2 followed by analysis of recovery of centromeric EGFP signals over time (arrowheads in D). (E) Quantification revealed rapid and quantitative recovery. Because dynamics and extent of recovery appeared indistinguishable during G1, S and G2 (see supplementary material Fig. S2B) data from experiments with bleaching at different cell cycle phases were aggregated. (F,G) Cenp-C-EGFP FRAP. Centromeric Cenp-C-EGFP in cells coexpressing mCherry-PCNA and HAnlsCycB$^{1–285}$-EBFP2 (not shown) was photobleached (circle in F) during G2 followed by analysis of recovery of centromeric EGFP signals over time (arrowheads in F). (G) Quantification revealed slow and partial recovery during all cell cycle phases. Dynamics and extent of recovery during G1, S and G2 was observed to be very similar (see supplementary material Fig. S2A). Thus data from experiments with bleaching at different cell cycle phases were aggregated.

observation further supports the proposal (Schittenhelm et al., 2010) that Cal1 functions as a Cid loading factor rather than as a structural stoichiometric link between Cid and Cenp-C.

Cenp-C is distinct from Cid and Cal1 with regard to mobility and time of centromere recruitment

Several observations have suggested that *Drosophila* Cenp-C might be intimately involved in Cid incorporation into the centromere. In syncytial embryos, Cenp-C and Cid incorporation were observed to be synchronous (Schuh et al., 2007). In addition, Cenp-C is required for normal levels of Cid and Cal1 at centromeres (Goshima et al., 2007; Erhardt et al., 2008; Schittenhelm et al., 2010). Moreover, overexpression of Cenp-C enhances excess incorporation of Cid into centromeres after co-overexpression of Cid and Cal1 (Schittenhelm et al., 2010). To compare the behavior of Cenp-C with that of Cid and Cal1 during progression of S2R+ cells through the cell cycle, we performed analyses with cells expressing EGFP-labeled Cenp-C in combination with mCherry-PCNA and HAnlsCycB$^{1–285}$-EBFP2. Quantification of total centromeric amounts after *in vivo* imaging revealed a statistically significant increase from late S to G2 phase. Moreover, the comparison of centromeric

Cenp-C-EGFP during G2 and G1 (Fig. 5C) confirmed that some incorporation of Cenp-C occurs also during mitosis (Fig. 3F) when taking the different centromere numbers in G2 and G1 into account. In addition, some incorporation might even occur from G1 to late S phase although the corresponding increase was not found to be statistically significant.

To analyze the mobility of centromeric Cenp-C-EGFP, we performed FRAP experiments (Fig. 5F,G). Some recovery of centromeric Cenp-C-EGFP signals after photobleaching was clearly observed. However, even during G2 where considerable incorporation of additional Cenp-C was found to occur (Fig. 5C), recovery was slow and partial (Fig. 5G). We could not detect significant differences in the rate of recovery between G2 and other cell cycle stages (supplementary material Fig. S2). In principle, the limited recovery after photobleaching might reflect either some low level dynamic exchange of centromeric Cenp-C or incorporation of additional Cenp-C into the centromere. In any case, our findings indicate that Cenp-C is far less dynamic than Cal1 and support the notion that Cenp-C functions as a stable docking platform for kinetochore proteins in mitosis and perhaps for Cal1 during Cid loading.

Discussion

Our results demonstrate that centromeric Cid behavior during progression through the cell division cycle is more complex than suggested so far. The 'loading only' model favored up to now is inadequate at least in case of *Drosophila* S2R+ cells. According to 'loading only', newly synthesized Cid is loaded onto centromeres during a defined window of the cell cycle and thereafter remains stably associated for many cell cycles. However, our data reveal, within one cell cycle, a succession of five different centromere states, of which some are characterized by turn-over or reduction in centromeric Cid. The five states are distinguished by the following features. (1) During early G1, when Cenp-C and still relatively high amounts of Cal1 are present at the centromere, loading of additional Cid into the centromere proceeds. (2) Towards the end of G1, when Cal1 levels are strongly reduced, centromeric deposition of Cid ceases. (3) Early in S phase, centromeric Cal1 levels are again high, but in contrast to early G1, this is not accompanied by additional centromeric Cid deposition or turnover. (4) However, starting in late S phase, in temporal correlation with centromere DNA replication (Sullivan and Karpen, 2001) and Cenp-C loading, incorporation of some newly synthesized Cid into the centromere, perhaps in exchange for old centromeric Cid, can be detected. (5) Finally, during metaphase of mitosis, Cid is recruited to centromeres resulting in an increase in total centromeric levels. However, this increase is only transient, because later at G1 onset, Cid levels are again equal to those just before mitosis.

The behavior of Cid in *Drosophila* S2R+ cells, as described here, is not identical to that proposed recently based on analyses in *Drosophila* S2 and Kc167 cells (Mellone et al., 2011). These latter two cell lines were proposed to incorporate additional Cid into centromeres only during metaphase followed by progression through interphase without any further Cid loading. Although our data fully agree on an occurrence of Cid recruitment to centromeres during metaphase, we found the associated increase in centromeric Cid levels to be transient and confined to mitosis. Moreover, we detected centromeric Cid deposition in interphase and a clear doubling of total centromeric Cid levels between early G1 and early S.

These apparent discrepancies might reflect real differences between the analyzed cell lines. However, the S2 and Kc167 data, which were obtained primarily from quench-chase-pulse experiments with SNAP-tagged Cid, does not rigorously exclude alternative interpretations that are consistent with the data from our FRAP analyses and microscopic quantification of total centromeric levels in combination with careful tracking of S2R+ cell cycle progression. The loading of Cid during G1 in S2R+ cells is quite slow, progressing gradually for 2–3 hours after completion of mitosis. Therefore, its detection is expected to be difficult by SNAP-tag labeling after brief chase periods, as applied by Mellone and colleagues (Mellone et al., 2011). With our S2R+ cells expressing SNAPf-tagged Cid, reproducible detection of low levels has proven to be difficult (data not shown). However, in contrast to G1 loading, all of the rapid recruitment in metaphase can occur during even brief chase periods, facilitating efficient detection by SNAP-tag labeling. We point out that, similar to the situation in S2R+ cells, Cid loading clearly occurs during G1 in mitotically proliferating cells in the central nervous system of the *Drosophila* larva (Dunleavy et al., 2012). Moreover, the analog of G1 loading is also observed in early *Drosophila* embryos where Cid loading occurs during anaphase of the extremely rapid, dramatically compressed cycles devoid of G phases (Schuh et al., 2007). Because loading during G1 has also been demonstrated for CENP-A in HeLa cells (Jansen et al., 2007; Hemmerich et al., 2008), it might represent an evolutionary conserved mode of loading in animal cells.

The prominent centromeric recruitment of Cid during metaphase in cultured *Drosophila* cells depends on Cyclin A degradation during early mitosis (Mellone et al., 2011). For unknown reasons, mitosis in cultured cells takes considerably longer than in the larval nervous system and in early embryos (Katsani et al., 2008; de Lartigue et al., 2011). It is possible therefore that degradation of Cyclin A is considerably advanced relative to the metaphase-to-anaphase transition in cultured cells compared with neuroblast and embryonic mitoses. Accordingly, early Cyclin A degradation might explain the more prominent centromeric recruitment of Cid before anaphase in cultured cells. Overall therefore, the reported diversity in Cid behavior in various *Drosophila* cell types (early embryos, larval CNS, cell lines) might not necessarily reflect differences in the proximal control of centromeric Cid dynamics but rather in upstream regulation of progression through the mitotic cell cycle. Nevertheless, meiotic Cid regulation in *Drosophila*, where additional Cid is stably incorporated during pre-meiotic G2 is clearly distinct from mitotic control (Dunleavy et al., 2012; Raychaudhuri et al., 2012).

A transient increase in centromeric CenH3 levels during mitosis has recently also been described in budding yeast (Shivaraju et al., 2012). In this case, the increase is observed during anaphase and is believed to be accompanied by a structural change in CenH3 nucleosomes. An octasome with two copies of CenH3 lacking Scm3 has been proposed to be present at the centromere during anaphase and a hemisome with one CenH3 copy and Scm3 outside anaphase, although not without conflicting evidence (Luconi et al., 2011; Xiao et al., 2011). Similarly, in human cells, a transition between CenH3 octasomes and hemisomes has been proposed to correlate with absence and presence of the Scm3 homolog HJURP, respectively

(Bui et al., 2012). In human cells, however, octasomes were proposed to be present in S phase and not during mitosis. Although in human cells many of these observations have also been questioned (Miell et al., 2013; Hasson et al., 2013; Padeganeh et al., 2013b), the possibility that different nucleosome structures could contribute to the different centromeric Cid states during the S2R+ cell cycle might deserve consideration.

Because *Drosophila* Cenp-C and Cal1 are clearly involved in the control of centromeric Cid (Schittenhelm et al., 2010; Goshima et al., 2007; Erhardt et al., 2008), we compared the behavior of these centromere proteins. In early embryos, the incorporation of additional Cenp-C occurs concomitant with Cid (Schuh et al., 2007). In S2R+ cells these two proteins behave differently. After a marginal increase during G1 where Cid loading occurs, centromeric Cenp-C amounts are raised primarily during late S, G2 and mitosis. According to FRAP analyses, a major fraction of centromeric Cenp-C is stable and a minor fraction is dynamic throughout interphase. In contrast to Cenp-C, all or at least the great majority of centromeric Cal1 turns over very rapidly. This result confirms the suggestions that Cal1 does function as a Cid loading factor rather than as a structural stable component of the centromere (Schittenhelm et al., 2010; Mellone et al., 2011; Phansalkar et al., 2012). Interestingly, our microscopic quantification of the amounts of Cal1 revealed a strong decrease during G1: the phase where Cal1 is proposed to be required for centromeric Cid deposition. Because Cid deposition starts in early G1 when Cal1 levels per genome equivalent are still high and since centromeric Cal1 is highly dynamic, this Cal1 decrease during G1 is not necessarily incompatible with the proposal that Cal1 functions as a Cid loading factor. In this case, the disappearance of Cal1 during G1 (possibly mediated by Cdh1-APC/C) might contribute to termination of Cid loading before the onset of S phase. We point out, however, that the reappearance of Cal1 around G1–S is not paralleled by Cid loading, indicating the existence of additional levels of control apart from Cal1 levels.

Our analyses implicate centromere DNA replication as an additional determinant of centromeric Cid behavior. Late in S phase, at the time when centromere DNA replication occurs in cultured *Drosophila* cells (Sullivan and Karpen, 2001), the high sensitivity of our FRAP experiments has uncovered a transition from a period without to a period with some recovery. Passage of a replication fork is thought to transiently remove nucleosomes from DNA (Corpet and Almouzni, 2009). Centromeric Cid nucleosomes might also dissociate during replication of the associated centromeric DNA, providing an opportunity for incorporation of newly synthesized Cid to a very limited extent. However, because recovery after Cid-EGFP photobleaching was observed to continue throughout G2, we assume that centromere DNA replication induces a distinct state in at least some of the centromeric Cid nucleosomes that endures beyond the actual replication of centromere DNA. A future careful analysis of the effects of DNA replication on centromeric Cid will clearly be of great interest. At least in mature sperm, Cenp-C and Cal1 are not present at the centromere (Raychaudhuri et al., 2012). Cid is the only known centromere protein present at sperm centromeres. Moreover, it is required for propagation of centromere identity (Raychaudhuri et al., 2012). It is conceivable therefore that apart from Cid, no other centromere-specific epigenetic marks are present in *Drosophila*. Accordingly, the fate of centromeric Cid during DNA replication would be of paramount importance for centromere maintenance.

In summary, beyond loading of additional Cid in G1, our findings also reveal distinct cell-cycle-dependent changes in centromeric Cid dynamics during mitosis and late S phase. Considering the importance of CenH3 for genetic stability, a future characterization of the corresponding molecular mechanisms should be of great interest.

Materials and Methods

Plasmids

The construct pMT-His2Av-mRFP-hygro contained the *Drosophila MtnA* promoter (−370 to +54) (Bunch et al., 1988) upstream of a *His2Av* gene version with a C-terminal mRFP extension. In addition, for selection of stable transformants, the construct included a selectable marker cassette with the copia promoter controlling a hygromycin phosphotransferase gene followed by an SV40 polyadenylation sequence. The selectable marker cassette was derived from pCoHygro (Invitrogen). The construct pMT-mCherry-PCNA-hygro contained the *MtnA* promoter upstream of an mCherry-PCNA fusion gene followed by the SV40 polyadenylation sequence. The PCNA sequence was isolated from pc1038-pENeGdPCNAL2 (Easwaran et al., 2007). In addition, the selectable marker cassette described above was present as well. The construct pCoPuro-MT-HAnlsCycB$^{1–285}$-EBFP2 contained the *MtnA* promoter upstream of an open reading frame coding for the HA epitope tag (HA), an SV40 nuclear localization signal (nls), a Cyclin B fragment (amino acids 1–285) and EBFP2 (Ai et al., 2007) followed by the SV40 polyadenylation sequence. In addition, the construct included the puromycin N-acetyltransferase gene under control of copia promoter for selection of stable transformants (Iwaki et al., 2003). The construct pCoBlast-giEGFP-cid was obtained by inserting the genomic *cid* region with an internal EGFP tag (Schuh et al., 2007) into pCoBlast (Invitrogen). For the generation of the construct pCoBlast-giSNAPf-cid the internal EGFP tag within pCoblast-giEGFP-cid was replaced by a SNAPf-encoding fragment (New England Biolabs). The construct pCoBlast-giEGFP-Cenp-C was generated by transferring a fragment (Schittenhelm et al., 2009) with the *Cenp-C* genomic region including an internal EGFP tag into pCoBlast. Similarly, the construct pCoBlast-gcal1-EGFP was generated by transferring the *cal1* genomic region with a C-terminal EGFP tag (Schittenhelm et al., 2010) into pCoBlast. Moreover, for the production of pCoblast-gEGFP-Bub3, the *Bub3* genomic region with an N-terminal EGFP tag (Pandey et al., 2007) was transferred into pCoBlast. Finally, the construct pCasper-gSpc25-EGFP-bla was obtained by replacing a *w* gene subfragment in pCaSpeR4-gSpc25-EGFP (Schittenhelm et al., 2007) with the selectable marker cassette containing a blasticidin S deaminase gene from pCoBlast. pCaSpeR-gSpc25-EGFP-bla was used for the generation of stable S2R+ cell lines expressing Spc25 with a C-terminal EGFP tag under control of the *Spc25* cis-regulatory sequences.

Cell culture

S2R+ cells were grown at 24℃ in Schneider's medium supplemented with 10% heat-inactivated fetal bovine serum, 100 units/ml penicillin and 100 µg/ml streptomycin (all from Gibco). For generation of stable lines, cells were transfected using FuGENE (Promega) with the constructs described above. Two days after transfection cells were split and grown in medium containing ~300 µg/ml hygromycin (Sigma) and/or 25 µg/ml blasticidin (Invitrogen) and/or 2 µg/ml puromycin (Gibco).

First, S2R+ cells were stably transfected with pMT-His2Av-mRFP-hygro. These cells expressed histone H2Av-mRFP at levels that were sufficient for microscopic detection even without induction of the *MtnA* promoter by $CuSO_4$ addition to the culture medium. These cells were stably transfected once more with a construct driving expression of an EGFP fusion (pCoBlast-giEGFP-cid, pCoBlast-giEGFP-CenpC, pCoBlast-gcal1-EGFP, pCoblast-gEGFP-Bub3 or pCaSpeR-gSpc25-EGFP-bla). Similarly, S2R+ cells expressing EGFP-labeled centromeric proteins in combination with mCherry-PCNA and HAnlsCycB$^{1–285}$-EBFP2 were generated by consecutive rounds of transfection and selection with the appropriate constructs (pCoBlast-giEGFP-cid, pCoBlast-giEGFP-CenpC or pCoBlast-gcal1-EGFP followed by pMT-mCherry-PCNA-hygro and pCoPuro-MT-HAnlsCycB$^{1–285}$-EBFP2). The expression of the cell cycle trackers (mCherry-PCNA and HAnlsCycB$^{1–285}$-EBFP2) was induced by addition of 300 µM $CuSO_4$ to the culture medium 24–48 hours before imaging.

For *in vivo* imaging, cells were plated in glass-bottom dishes (Greiner Bio-One GmbH). For immunofluorescence experiments, cells were plated in culture dishes with glass coverslips. For live imaging and staining, 2- to 3-day-old subconfluent monolayers were used.

Cell labeling and quantitative analysis with fixed cells

SNAP-Cell TMR-Star (New England Biolabs) was used for labeling of Cid-SNAPf. The compound was added to the medium (final concentration 3 µM) for

20 minutes at 24℃. Thereafter, cells were washed three times with conditioned medium before EdU pulse labeling (Salic and Mitchison, 2008). EdU (Life Technologies) was added to the medium (final concentration 5 µM) for 30 minutes at 24℃. Cells were fixed in 4% formaldehyde, 0.1% Triton X-100 in phosphate-buffered saline (PBS: 137 mM NaCl, 2.7 mM KCl, 1.47 mM KH_2PO_4, 6.46 mM Na_2HPO_4, pH 7.4) for 20 minutes, rinsed with PBS and permeabilized with 0.5% Triton X-100 in PBS for 20 minutes. Coverslips were briefly rinsed and then washed twice for 5 minutes with PBS. Before anti-cyclin-B staining, cells were incubated in blocking solution (1% FBS in PBS) for 30 minutes. Incubation with rabbit anti-cyclin-B (1:2000) (Jacobs et al., 1998) was performed for 1 hour in blocking solution, as was incubation with Cy5-conjugated goat anti-rabbit (Jackson Immunochemicals) (1:500). Both incubations were followed by three washes for 5 minutes each with blocking solution. Coverslips were further processed using the Click-iT EdU Alexa Fluor 488 Imaging Kit (Life Technologies), stained with Hoechst 33258 at 1 µg/ml for 30 minutes in PBS and mounted in 70% glycerol, 50 mM Tris-HCl, pH 8.5, 5 mM *p*-phenylenediamine and 50 mM *n*-propylgallate. All incubations were carried out at room temperature in the dark. Samples were imaged with a laser-scanning confocal microscope (Olympus FV1000) equipped with 60×, 1.35 NA oil objective using excitation at 405 nm for Hoechst 33258, 488 nm for Alexa Fluor 488, 559 nm for TMR and 635 nm for Cy5. The pinhole was set to 300 µm. Stacks with 20 sections and 0.5 µm spacing were projected with Fiji (Schindelin et al., 2012) to reduce dimensionality for CellProfiler analysis. Maximum projections were used for image clusterization and the corresponding average projections for intensity quantification. Briefly, nuclei were identified based on the DNA staining. Nuclei were assigned to either the 'S' or the 'not S' subgroups based on presence or absence of EdU signals within the nuclear area. S-phase nuclei were further separated into 'early S' and 'mid/late S' based on the relative nuclear area occupied by the EdU labeling. If the EdU-labeled region was either more or less than 35% of the nuclear area, nuclei were classified as either 'early S' or 'mid/late S', respectively. Based on anti-cyclin-B signal intensities below or above a threshold value, 'not S' cells were further divided into 'G1' or 'G2' subgroups, respectively. The anti-cyclin B signal threshold value was determined for each experiment individually based on the signals present in 'S' cells. Centromeres were identified as intranuclear regions with the brightest TMR signals using an intensity threshold adjusted manually in each experiment. The identified potential centromeres were filtered by size, excluding objects that were too big or too small. The areas of the selected regions were further increased by including a surrounding rim with the width of one pixel to incorporate all of the centromeric signal. The TMR intensity values within these enlarged regions were integrated, followed by background subtraction to arrive at a measure for centromeric Cid-SNAPf levels. For this background subtraction, we determined an average background intensity per pixel after quantification of intensities in the TMR channel within the whole nuclear area excluding the centromere region. We note that with some exceptional cell batches, we observed that Cid-SNAPf levels were slightly but significantly higher in G2 compared with S (data not shown). The violin plots were produced in R (R Development Core Team) with violinmplot library. *P*-values are from Student's *t*-tests.

Live imaging

Live imaging was carried out using either wide-field or laser-scanning confocal microscopy. Wide-field microscopy was performed with a Zeiss Cell Observer HS system equipped with a 470 nm (GFP) and a 555 nm (mRFP) light-emitting diode (LED) as fast-switchable light sources. The 555 nm LED was used in combination with a 550/32 bandpass filter. Emitted signals were detected with a dual band-pass filter (Zeiss 56HE without excitation filter). A 63×, 1.4 NA oil-immersion objective was used. Number of focal planes per time point, as well as time intervals and total duration of the *in vivo* imaging, were adjusted according to experimental needs. The spacing of focal planes was 0.7 µm in all experiments. For laser-scanning confocal microscopy, we used the set-up described above with Nomarski DIC detection instead of the 635 nm diode laser channel. The zoom was selected according to the experimental needs.

Quantitative analysis after live imaging

In general, quantifications of fluorescent signal intensities in time-lapse movies were performed using ImageJ and Fiji. Calculations were performed using Microsoft Excel. All quantifications were performed after average projection of z stacks. For quantification of centromeric Cid and Cenp-C signal intensities, core centromeric regions were identified initially as the brightest spots within the cell nucleus by applying manually adjusted thresholds. These core regions were further expanded by a surrounding band with the width of 4 pixels to ensure complete coverage of centromeric signals. For background subtraction, an additional rim of 4 pixels width was selected around the expanded centromeric regions. Average pixel intensities in these outer rims were determined and used for background correction of the intensity values within the expanded centromeric regions.

We emphasize that the total size of the selected centromeric regions represented an area fraction that remained comparable at the different time points during progression through the cell cycle, including the mitotic stages where centromere clustering changed dramatically. To exclude potential quantification artifacts caused by substantial drift of centromere positions along the *z*-axis, all movies in which such out-of-focus movement was apparent were omitted from further analysis. The intensity changes over time that we have determined, therefore, do not simply reflect changes in the spatial organization of centromeres.

After imaging with the wide-field set-up, correction for photobleaching was performed when quantifying signals during progression through mitosis and G1. For this correction, centromeric intensities in three interphase cells that were neighbors of a given mitotic or G1 cell were quantified. The decline of signal intensity in these interphase cells over time was assumed to reflect photobleaching. The centromeric intensities in the three interphase cells in the first frame were set to 1, and the accordingly aligned three intensity curves were averaged before extraction of a slope that was used for correction of signal bleaching in the mitotic or G1 cells. After confocal microscopy, such correction was omitted because significant photobleaching was not detected in neighboring interphase cells with the applied settings. Photobleaching-corrected wide-field and non-corrected confocal data for centromeric Cid-EGFP intensities extracted from movies covering late G2, mitosis and G1 (Fig. 2C) were found to be in excellent agreement.

Quantification of Cal1-EGFP was performed after laser-scanning confocal microscopy. Still frames from a representative movie after de-noising and maximum projection of *z* stacks are shown in Fig. 5A. As explained in the main text, centromeric and nucleolar Cal1-EGFP were quantified together during progression through the cell cycle. The high turnover of centromeric Cal1-EGFP revealed by our FRAP analyses (Fig. 5D,E) supports the assumption that nucleolar and centromeric Cal1 pools undergo rapid exchange. Centromeric and nucleolar regions were manually selected in average projected movies. Subtraction of local background was performed with use of manually selected surrounding regions. Before averaging, the resulting curves of Cal1-EGFP intensities over time were normalized and aligned by setting the G2 values to 1. The values displayed in the bar diagram (Fig. 5C) were obtained as explained in the legend of Fig. 2A,B.

FRAP

FRAP experiments were performed with the confocal laser-scanning microscope using the 488 nm and 559 nm diode lasers. Three to five images were taken before bleaching of centromere clusters (pre-bleach). Bleaching was carried out with the 405 nm laser and the SIM-scanner. To evaluate the exchange of centromeric Cenp-C, small centromere clusters were usually chosen for FRAP analysis to minimize the bleaching of Cenp-C-EGFP to a minor fraction of the total cellular pool. Therefore, absence of fluorescent Cenp-C-EGFP can be discounted as explanation for the observed incomplete recovery of centromeric Cenp-C-EGFP after photobleaching. For the analysis of centromeric Cal1-EGFP, we selected those cells that had centromere clusters well separated from nucleoli before bleaching the centromeric region in order to minimize the fraction of total cellular Cal1-EGFP that was photobleached. In FRAP analyses with Cid-EGFP, both small and large centromere clusters were photobleached. Both analyses gave comparative results (data not shown), indicating that the observed recovery reflects recruitment of newly synthesized Cid-EGFP rather than exchange between different centromeres.

To maximize image acquisition speed during the recovery phase after the initial photobleaching pulse, a limited region around the bleached area was imaged. The acquired *z* stacks were further processed with ImageJ and Fiji. Centromeric signals were quantified in average projections and local background values were subtracted (see above). Moreover, we corrected for the unintended but unavoidable photobleaching caused by imaging during the recovery phase as follows. In case of Cid-EGFP and Cenp-C-EGFP, centromeric signal intensities of centromere clusters in the same or in neighboring cells that had not been exposed to the initial photobleaching pulse were quantified during the recovery phase. The intensity decrease of these signals was assumed to reflect photobleaching caused by imaging during the recovery phase. The rate of decrease was determined and used for correction (see above). With Cal1-EGFP, the nucleolar signals within the cell in which a well-separated centromere cluster had been bleached during the initial photo pulse was used to correct for bleaching caused by imaging during the recovery phase. To compare FRAP data from different cells for Cenp-C-EGFP and Cal1-EGFP, corrected curves were transformed by setting the centromeric signal intensities before the initial photobleaching pulse (pre-bleach) to one and adjusting all other intensity values proportionally. The local regression curves in Fig. 5E,G were produced using lowess smoothing with the R software package. For Cid-EGFP, pre-bleach values were also set to one. However, the post-bleach value obtained immediately after the initial photobleaching pulse was set to zero for each curve. Therefore, the curves displayed for Cid-EGFP (Fig. 4) indicate the proportion of recovery of the initially photobleached material over time.

Acknowledgements

We thank Martina Trost for her help during plasmid constructions, as well as during cell line generation and maintenance. We thank Mark D. Robinson for his expert assistance with statistical analyses.

Author contributions

C.F.L. and P.V.L. conceived and designed the experiments. P.V.L. performed the experiments. C.F.L. and P.V.L. analyzed the data. F.S. contributed essential reagents. P.V.L. and C.F.L. wrote the paper.

Funding

This work was supported by grants from the Swiss National Science Foundation. Some results were analyzed using IGB RAS equipment supported by the Ministry of Science and Education of the Russian Federation [grant number 16.552.11.7067]. The funders had no role in study design, data collection and analysis, decision to publish or preparation of the manuscript.

Supplementary material available online at
http://jcs.biologists.org/lookup/suppl/doi:10.1242/jcs.134122/-/DC1

References

Ai, H. W., Shaner, N. C., Cheng, Z., Tsien, R. Y. and Campbell, R. E. (2007). Exploration of new chromophore structures leads to the identification of improved blue fluorescent proteins. *Biochemistry* **46**, 5904-5910.

Alonso, A., Hasson, D., Cheung, F. and Warburton, P. E. (2010). A paucity of heterochromatin at functional human neocentromeres. *Epigenetics Chromatin* **3**, 6.

Amor, D. J., Bentley, K., Ryan, J., Perry, J., Wong, L., Slater, H. and Choo, K. H. (2004). Human centromere repositioning "in progress". *Proc. Natl. Acad. Sci. USA* **101**, 6542-6547.

Barry, A. E., Howman, E. V., Cancilla, M. R., Saffery, R. and Choo, K. H. (1999). Sequence analysis of an 80 kb human neocentromere. *Hum. Mol. Genet.* **8**, 217-227.

Basu, J., Logarinho, E., Herrmann, S., Bousbaa, H., Li, Z., Chan, G. K., Yen, T. J., Sunkel, C. E. and Goldberg, M. L. (1998). Localization of the Drosophila checkpoint control protein Bub3 to the kinetochore requires Bub1 but not Zw10 or Rod. *Chromosoma* **107**, 376-385.

Black, B. E. and Cleveland, D. W. (2011). Epigenetic centromere propagation and the nature of CENP-a nucleosomes. *Cell* **144**, 471-479.

Blower, M. D. and Karpen, G. H. (2001). The role of Drosophila CID in kinetochore formation, cell-cycle progression and heterochromatin interactions. *Nat. Cell Biol.* **3**, 730-739.

Bui, M., Dimitriadis, E. K., Hoischen, C., An, E., Quénet, D., Giebe, S., Nita-Lazar, A., Diekmann, S. and Dalal, Y. (2012). Cell-cycle-dependent structural transitions in the human CENP-A nucleosome in vivo. *Cell* **150**, 317-326.

Bunch, T. A., Grinblat, Y. and Goldstein, L. S. B. (1988). Characterization and use of the Drosophila metallothionein promoter in cultured Drosophila melanogaster cells. *Nucleic Acids Res.* **16**, 1043-1061.

Camahort, R., Li, B., Florens, L., Swanson, S. K., Washburn, M. P. and Gerton, J. L. (2007). Scm3 is essential to recruit the histone h3 variant cse4 to centromeres and to maintain a functional kinetochore. *Mol. Cell* **26**, 853-865.

Carpenter, A. E., Jones, T. R., Lamprecht, M. R., Clarke, C., Kang, I. H., Friman, O., Guertin, D. A., Chang, J. H., Lindquist, R. A., Moffat, J. et al. (2006). CellProfiler: image analysis software for identifying and quantifying cell phenotypes. *Genome Biol.* **7**, R100.

Carroll, C. W., Silva, M. C., Godek, K. M., Jansen, L. E. and Straight, A. F. (2009). Centromere assembly requires the direct recognition of CENP-A nucleosomes by CENP-N. *Nat. Cell Biol.* **11**, 896-902.

Corpet, A. and Almouzni, G. (2009). Making copies of chromatin: the challenge of nucleosomal organization and epigenetic information. *Trends Cell Biol.* **19**, 29-41.

Dambacher, S., Deng, W., Hahn, M., Sadic, D., Fröhlich, J., Nuber, A., Hoischen, C., Diekmann, S., Leonhardt, H. and Schotta, G. (2012). CENP-C facilitates the recruitment of M18BP1 to centromeric chromatin. *Nucleus* **3**, 101-110.

de Lartigue, J., Brust-Mascher, I. and Scholey, J. M. (2011). Anaphase B spindle dynamics in Drosophila S2 cells: Comparison with embryo spindles. *Cell Div.* **6**, 8.

Dechassa, M. L., Wyns, K., Li, M., Hall, M. A., Wang, M. D. and Luger, K. (2011). Structure and Scm3-mediated assembly of budding yeast centromeric nucleosomes. *Nat. Commun.* **2**, 313.

du Sart, D., Cancilla, M. R., Earle, E., Mao, J. I., Saffery, R., Tainton, K. M., Kalitsis, P., Martyn, J., Barry, A. E. and Choo, K. H. (1997). A functional neo-centromere formed through activation of a latent human centromere and consisting of non-alpha-satellite DNA. *Nat. Genet.* **16**, 144-153.

Dunleavy, E. M., Roche, D., Tagami, H., Lacoste, N., Ray-Gallet, D., Nakamura, Y., Daigo, Y., Nakatani, Y. and Almouzni-Pettinotti, G. (2009). HJURP is a cell-cycle-dependent maintenance and deposition factor of CENP-A at centromeres. *Cell* **137**, 485-497.

Dunleavy, E. M., Beier, N. L., Gorgescu, W., Tang, J., Costes, S. V. and Karpen, G. H. (2012). The cell cycle timing of centromeric chromatin assembly in Drosophila meiosis is distinct from mitosis yet requires CAL1 and CENP-C. *PLoS Biol.* **10**, e1001460.

Earnshaw, W. C. and Rothfield, N. (1985). Identification of a family of human centromere proteins using autoimmune sera from patients with scleroderma. *Chromosoma* **91**, 313-321.

Earnshaw, W. C., Allshire, R. C., Black, B. E., Bloom, K., Brinkley, B. R., Brown, W., Cheeseman, I. M., Choo, K. H., Copenhaver, G. P., Deluca, J. G. et al. (2013). Esperanto for histones: CENP-A, not CenH3, is the centromeric histone H3 variant. *Chromosome Res.* **21**, 101-106.

Easwaran, H. P., Leonhardt, H. and Cardoso, M. C. (2007). Distribution of DNA replication proteins in Drosophila cells. *BMC Cell Biol.* **8**, 42.

Erhardt, S., Mellone, B. G., Betts, C. M., Zhang, W., Karpen, G. H. and Straight, A. F. (2008). Genome-wide analysis reveals a cell cycle-dependent mechanism controlling centromere propagation. *J. Cell Biol.* **183**, 805-818.

Foltz, D. R., Jansen, L. E., Bailey, A. O., Yates, J. R., 3rd, Bassett, E. A., Wood, S., Black, B. E. and Cleveland, D. W. (2009). Centromere-specific assembly of CENP-a nucleosomes is mediated by HJURP. *Cell* **137**, 472-484.

Fujita, Y., Hayashi, T., Kiyomitsu, T., Toyoda, Y., Kokubu, A., Obuse, C. and Yanagida, M. (2007). Priming of centromere for CENP-A recruitment by human hMis18alpha, hMis18beta, and M18BP1. *Dev. Cell* **12**, 17-30.

Gascoigne, K. E., Takeuchi, K., Suzuki, A., Hori, T., Fukagawa, T. and Cheeseman, I. M. (2011). Induced ectopic kinetochore assembly bypasses the requirement for CENP-A nucleosomes. *Cell* **145**, 410-422.

Goshima, G., Wollman, R., Goodwin, S. S., Zhang, N., Scholey, J. M., Vale, R. D. and Stuurman, N. (2007). Genes required for mitotic spindle assembly in Drosophila S2 cells. *Science* **316**, 417-421.

Hasson, D., Panchenko, T., Salimian, K. J., Salman, M. U., Sekulic, N., Alonso, A., Warburton, P. E. and Black, B. E. (2013). The octamer is the major form of CENP-A nucleosomes at human centromeres. *Nat. Struct. Mol. Biol.* **20**, 687-695.

Hayashi, T., Fujita, Y., Iwasaki, O., Adachi, Y., Takahashi, K. and Yanagida, M. (2004). Mis16 and Mis18 are required for CENP-A loading and histone deacetylation at centromeres. *Cell* **118**, 715-729.

Heeger, S., Leismann, O., Schittenhelm, R., Schraidt, O., Heidmann, S. and Lehner, C. F. (2005). Genetic interactions of separase regulatory subunits reveal the diverged Drosophila Cenp-C homolog. *Genes Dev.* **19**, 2041-2053.

Hemmerich, P., Weidtkamp-Peters, S., Hoischen, C., Schmiedeberg, L., Erliandri, I. and Diekmann, S. (2008). Dynamics of inner kinetochore assembly and maintenance in living cells. *J. Cell Biol.* **180**, 1101-1114.

Henikoff, S., Ahmad, K., Platero, J. S. and van Steensel, B. (2000). Heterochromatic deposition of centromeric histone H3-like proteins. *Proc. Natl. Acad. Sci. USA* **97**, 716-721.

Heun, P., Erhardt, S., Blower, M. D., Weiss, S., Skora, A. D. and Karpen, G. H. (2006). Mislocalization of the Drosophila centromere-specific histone CID promotes formation of functional ectopic kinetochores. *Dev. Cell* **10**, 303-315.

Hewawasam, G., Shivaraju, M., Mattingly, M., Venkatesh, S., Martin-Brown, S., Florens, L., Workman, J. L. and Gerton, J. L. (2010). Psh1 is an E3 ubiquitin ligase that targets the centromeric histone variant Cse4. *Mol. Cell* **40**, 444-454.

Iwaki, T., Figuera, M., Ploplis, V. A. and Castellino, F. J. (2003). Rapid selection of Drosophila S2 cells with the puromycin resistance gene. *Biotechniques* **35**, 482-484, 486.

Jacobs, H. W., Knoblich, J. A. and Lehner, C. F. (1998). Drosophila Cyclin B3 is required for female fertility and is dispensable for mitosis like Cyclin B. *Genes Dev.* **12**, 3741-3751.

Janke, C., Ortiz, J., Lechner, J., Shevchenko, A., Shevchenko, A., Magiera, M. M., Schramm, C. and Schiebel, E. (2001). The budding yeast proteins Spc24p and Spc25p interact with Ndc80p and Nuf2p at the kinetochore and are important for kinetochore clustering and checkpoint control. *EMBO J.* **20**, 777-791.

Jansen, L. E., Black, B. E., Foltz, D. R. and Cleveland, D. W. (2007). Propagation of centromeric chromatin requires exit from mitosis. *J. Cell Biol.* **176**, 795-805.

Katsani, K. R., Karess, R. E., Dostatni, N. and Doye, V. (2008). In vivo dynamics of Drosophila nuclear envelope components. *Mol. Biol. Cell* **19**, 3652-3666.

Keppler, A., Kindermann, M., Gendreizig, S., Pick, H., Vogel, H. and Johnsson, K. (2004). Labeling of fusion proteins of O6-alkylguanine-DNA alkyltransferase with small molecules in vivo and in vitro. *Methods* **32**, 437-444.

Kingston, I. J., Yung, J. S. and Singleton, M. R. (2011). Biophysical characterization of the centromere-specific nucleosome from budding yeast. *J. Biol. Chem.* **286**, 4021-4026.

Lagana, A., Dorn, J. F., De Rop, V., Ladouceur, A. M., Maddox, A. S. and Maddox, P. S. (2010). A small GTPase molecular switch regulates epigenetic centromere maintenance by stabilizing newly incorporated CENP-A. *Nat. Cell Biol.* **12**, 1186-1193.

Lehner, C. F. and O'Farrell, P. H. (1990). The roles of Drosophila cyclins A and B in mitotic control. *Cell* **61**, 535-547.

Leonhardt, H., Rahn, H. P., Weinzierl, P., Sporbert, A., Cremer, T., Zink, D. and Cardoso, M. C. (2000). Dynamics of DNA replication factories in living cells. *J. Cell Biol.* **149**, 271-280.

Lermontova, I., Schubert, V., Fuchs, J., Klatte, S., Macas, J. and Schubert, I. (2006). Loading of Arabidopsis centromeric histone CENH3 occurs mainly during G2 and requires the presence of the histone fold domain. *Plant Cell* **18**, 2443-2451.

Luconi, L., Araki, Y., Erlemann, S. and Schiebel, E. (2011). The CENP-A chaperone Scm3 becomes enriched at kinetochores in anaphase independently of CENP-A incorporation. *Cell Cycle* **10**, 3369-3378.

McAinsh, A. D. and Meraldi, P. (2011). The CCAN complex: linking centromere specification to control of kinetochore-microtubule dynamics. *Semin. Cell Dev. Biol.* **22**, 946-952.

Mellone, B. G., Grive, K. J., Shteyn, V., Bowers, S. R., Oderberg, I. and Karpen, G. H. (2011). Assembly of Drosophila centromeric chromatin proteins during mitosis. *PLoS Genet.* **7**, e1002068.

Mendiburo, M. J., Padeken, J., Fülöp, S., Schepers, A. and Heun, P. (2011). Drosophila CENH3 is sufficient for centromere formation. *Science* **334**, 686-690.

Miell, M. D. D., Fuller, C. J., Guse, A., Barysz, H. M., Downes, A., Owen-Hughes, T., Rappsilber, J., Straight, A. F. and Allshire, R. C. (2013). CENP-A confers a reduction in height on octameric nucleosomes. *Nat. Struct. Mol. Biol.* **20**, 763-765.

Mizuguchi, G., Xiao, H., Wisniewski, J., Smith, M. M. and Wu, C. (2007). Nonhistone Scm3 and histones CenH3-H4 assemble the core of centromere-specific nucleosomes. *Cell* **129**, 1153-1164.

Moore, L. L. and Roth, M. B. (2001). HCP-4, a CENP-C-like protein in Caenorhabditis elegans, is required for resolution of sister centromeres. *J. Cell Biol.* **153**, 1199-1208.

Moree, B., Meyer, C. B., Fuller, C. J. and Straight, A. F. (2011). CENP-C recruits M18BP1 to centromeres to promote CENP-A chromatin assembly. *J. Cell Biol.* **194**, 855-871.

Moreno-Moreno, O., Torras-Llort, M. and Azorín, F. (2006). Proteolysis restricts localization of CID, the centromere-specific histone H3 variant of Drosophila, to centromeres. *Nucleic Acids Res.* **34**, 6247-6255.

Moreno-Moreno, O., Medina-Giró, S., Torras-Llort, M. and Azorín, F. (2011). The F box protein partner of paired regulates stability of Drosophila centromeric histone H3, CenH3(CID). *Curr. Biol.* **21**, 1488-1493.

Nechemia-Arbely, Y., Fachinetti, D. and Cleveland, D. W. (2012). Replicating centromeric chromatin: spatial and temporal control of CENP-A assembly. *Exp. Cell Res.* **318**, 1353-1360.

Olszak, A. M., van Essen, D., Pereira, A. J., Diehl, S., Manke, T., Maiato, H., Saccani, S. and Heun, P. (2011). Heterochromatin boundaries are hotspots for de novo kinetochore formation. *Nat. Cell Biol.* **13**, 799-808.

Padeganeh, A., De Rop, V. and Maddox, P. S. (2013a). Nucleosomal composition at the centromere: a numbers game. *Chromosome Res.* **21**, 27-36.

Padeganeh, A., Ryan, J., Boisvert, J., Ladouceur, A. M., Dorn, J. F. and Maddox, P. S. (2013b). Octameric CENP-A nucleosomes are present at human centromeres throughout the cell cycle. *Curr. Biol.* **23**, 764-769.

Pandey, R., Heeger, S. and Lehner, C. F. (2007). Rapid effects of acute anoxia on spindle kinetochore interactions activate the mitotic spindle checkpoint. *J. Cell Sci.* **120**, 2807-2818.

Perpelescu, M. and Fukagawa, T. (2011). The ABCs of CENPs. *Chromosoma* **120**, 425-446.

Perpelescu, M., Nozaki, N., Obuse, C., Yang, H. and Yoda, K. (2009). Active establishment of centromeric CENP-A chromatin by RSF complex. *J. Cell Biol.* **185**, 397-407.

Phansalkar, R., Lapierre, P. and Mellone, B. G. (2012). Evolutionary insights into the role of the essential centromere protein CAL1 in Drosophila. *Chromosome Res.* **20**, 493-504.

Przewloka, M. R., Venkei, Z., Bolanos-Garcia, V. M., Debski, J., Dadlez, M. and Glover, D. M. (2011). CENP-C is a structural platform for kinetochore assembly. *Curr. Biol.* **21**, 399-405.

Ranjitkar, P., Press, M. O., Yi, X., Baker, R., MacCoss, M. J. and Biggins, S. (2010). An E3 ubiquitin ligase prevents ectopic localization of the centromeric histone H3 variant via the centromere targeting domain. *Mol. Cell* **40**, 455-464.

Raychaudhuri, N., Dubruille, R., Orsi, G. A., Bagheri, H. C., Loppin, B. and Lehner, C. F. (2012). Transgenerational propagation and quantitative maintenance of paternal centromeres depends on Cid/Cenp-A presence in Drosophila sperm. *PLoS Biol.* **10**, e1001434.

Salic, A. and Mitchison, T. J. (2008). A chemical method for fast and sensitive detection of DNA synthesis in vivo. *Proc. Natl. Acad. Sci. USA* **105**, 2415-2420.

Sanchez-Pulido, L., Pidoux, A. L., Ponting, C. P. and Allshire, R. C. (2009). Common ancestry of the CENP-A chaperones Scm3 and HJURP. *Cell* **137**, 1173-1174.

Schindelin, J., Arganda-Carreras, I., Frise, E., Kaynig, V., Longair, M., Pietzsch, T., Preibisch, S., Rueden, C., Saalfeld, S., Schmid, B. et al. (2012). Fiji: an open-source platform for biological-image analysis. *Nat. Methods* **9**, 676-682.

Schittenhelm, R. B., Heeger, S., Althoff, F., Walter, A., Heidmann, S., Mechtler, K. and Lehner, C. F. (2007). Spatial organization of a ubiquitous eukaryotic kinetochore protein network in Drosophila chromosomes. *Chromosoma* **116**, 385-402.

Schittenhelm, R. B., Chaleckis, R. and Lehner, C. F. (2009). Essential functional domains and intrakinetochore localization of Drosophila Spc105. *EMBO J.* **28**, 2374-2386.

Schittenhelm, R. B., Althoff, F., Heidmann, S. and Lehner, C. F. (2010). Detrimental incorporation of excess Cenp-A/Cid and Cenp-C into Drosophila centromeres is prevented by limiting amounts of the bridging factor Cal1. *J. Cell Sci.* **123**, 3768-3779.

Schuh, M., Lehner, C. F. and Heidmann, S. (2007). Incorporation of Drosophila CID/CENP-A and CENP-C into centromeres during early embryonic anaphase. *Curr. Biol.* **17**, 237-243.

Shermoen, A. W., McCleland, M. L. and O'Farrell, P. H. (2010). Developmental control of late replication and S phase length. *Curr. Biol.* **20**, 2067-2077.

Shivaraju, M., Unruh, J. R., Slaughter, B. D., Mattingly, M., Berman, J. and Gerton, J. L. (2012). Cell-cycle-coupled structural oscillation of centromeric nucleosomes in yeast. *Cell* **150**, 304-316.

Silva, M. C. C., Bodor, D. L., Stellfox, M. E., Martins, N. M., Hochegger, H., Foltz, D. R. and Jansen, L. E. (2012). Cdk activity couples epigenetic centromere inheritance to cell cycle progression. *Dev. Cell* **22**, 52-63.

Sullivan, B. and Karpen, G. (2001). Centromere identity in Drosophila is not determined in vivo by replication timing. *J. Cell Biol.* **154**, 683-690.

Tachiwana, H., Kagawa, W., Shiga, T., Osakabe, A., Miya, Y., Saito, K., Hayashi-Takanaka, Y., Oda, T., Sato, M., Park, S. Y. et al. (2011). Crystal structure of the human centromeric nucleosome containing CENP-A. *Nature* **476**, 232-235.

Takayama, Y., Sato, H., Saitoh, S., Ogiyama, Y., Masuda, F. and Takahashi, K. (2008). Biphasic incorporation of centromeric histone CENP-A in fission yeast. *Mol. Biol. Cell* **19**, 682-690.

Taylor, S. S., Ha, E. and McKeon, F. (1998). The human homologue of Bub3 is required for kinetochore localization of Bub1 and a Mad3/Bub1-related protein kinase. *J. Cell Biol.* **142**, 1-11.

Wigge, P. A. and Kilmartin, J. V. (2001). The Ndc80p complex from Saccharomyces cerevisiae contains conserved centromere components and has a function in chromosome segregation. *J. Cell Biol.* **152**, 349-360.

Xiao, H., Mizuguchi, G., Wisniewski, J., Huang, Y., Wei, D. and Wu, C. (2011). Nonhistone Scm3 binds to AT-rich DNA to organize atypical centromeric nucleosome of budding yeast. *Mol. Cell* **43**, 369-380.